

A search for high-mass black holes in data from the second LIGO observing run using a Bayesian ranking-statistic

A. Vajpeyi,^{1,2} R. Smith,^{1,2} E. Thrane,^{1,2} G. Ashton,^{1,2} T. Alford,³
S. Garza,³ M. Isi,^{4,5} J. Kanner,³ T.J. Massinger,³ and L. Xiao³

¹*School of Physics and Astronomy, Monash University, Clayton VIC 3800, Australia*

²*OzGrav: The ARC Centre of Excellence for Gravitational Wave Discovery, Clayton VIC 3800, Australia*

³*LIGO Laboratory, California Institute of Technology, Pasadena, CA 91125, USA*

⁴*LIGO Laboratory, Massachusetts Institute of Technology, Cambridge, MA 02139, USA*

⁵*Department of Physics and Kavli Institute for Astrophysics and Space Research,
Massachusetts Institute of Technology, 77 Massachusetts Ave, Cambridge, MA 02139, USA*

(Dated: May 26, 2021)

The detection of an intermediate-mass black hole population ($10^2 - 10^6 M_\odot$) will provide probes to their formation environments (e.g., disks of active galactic nuclei, globular clusters) and illuminate a potential pathway to produce supermassive black holes. Numerous methods to search for $10^4 - 10^6 M_\odot$ intermediate-mass black holes exist, while the primary method to find $10^2 - 10^3 M_\odot$ is by identifying gravitational-waves emitted from the merger of stellar binaries. Ground-based gravitational-wave detectors are in principle sensitive to such mergers and have found one $142^{+28}_{-16} M_\odot$ intermediate-mass black hole. In reality, ground-based detectors are plagued with short-duration instrumental transients that mimic the gravitational-wave signals from mergers capable of producing intermediate-mass black holes, making their detection difficult. Here we demonstrate a ranking statistic utilizing Bayesian inference to detect high-mass binary black hole mergers (with a total mass $> 55 M_\odot$). We apply this technique to the high-mass triggers during LIGO's second observing run to search for previously unresolved gravitational-wave signals from high-mass binary black holes. Our analysis does not discover new intermediate-mass black holes. However, we find support for some stellar mass binary black holes unreported in GWTC-1.

I. INTRODUCTION

Since the 1970s, there has been a steady accumulation of evidence for stellar mass ($M_{\text{BH}} < 10^2 M_\odot$) and supermassive black holes ($M_{\text{BH}} > 10^6 M_\odot$) [1–7]. However, there is a deficiency of observational evidence for black holes in the ‘intermediate-mass’ range $10^2 - 10^6 M_\odot$. The discovery of an intermediate-mass black hole population will bridge this observational gap, probe intermediate-mass formation environments (e.g. accretion disks of active galactic nuclei [8–20], the centers of dense stellar clusters [21–31], Population-III stars [32–36]), and illuminate our understanding of supermassive black hole formation [37–40]. A variety of techniques have been employed to search for $10^4 - 10^6 M_\odot$ intermediate mass candidates (reverberation mapping [41], direct kinematic measurements [42, 43], applying macroscopic galaxy to black hole mass scaling relations ($M_{\text{BH}}-\sigma$ and $M_{\text{BH}}-L$ relations) [44, 45], studying X-ray luminosity and spectra [46, 47], gravitational lensing of light curves [48], and others [49–51]). However, these observational techniques are challenging to use for intermediate mass black holes due to their small sphere of influence compared to super-massive black holes [51]. Additionally, some candidates discovered with these techniques can be attributed to sources without intermediate-mass black holes (e.g. clusters of stellar-mass black holes [52, 53], anisotropic emission from neutron stars [54, 55]), while others have high uncertainties due to the observational techniques utilized [49].

Compact binaries coalescences (CBCs) can provide un-

ambiguous gravitational-wave signals for intermediate-mass candidates (e.g. the $142^{+28}_{-16} M_\odot$ remnant observed from the gravitational wave event GW190521 [56]). Ground-based gravitational wave detectors can probe the lower-end $10^2 - 10^3 M_\odot$ of the intermediate mass range. As a binary’s total mass M_T is associated with its gravitational-wave merger frequency, $f \sim M_T^{-1}$, systems with large M_T have very low merger frequencies $f < 100$ Hz. Hence, ground based gravitational wave detectors ($\sim 10^1 - 10^3$ Hz) are sensitive to the last milliseconds of merging systems with $100 M_\odot < M_T < 400 M_\odot$ [57–59], while space-based detectors ($\sim 10^{-2} - 10^1$ Hz) can study the full signals of merging systems with $10^4 M_\odot < M_T < 10^7 M_\odot$ [59, 60].

Because of the short-duration of intermediate-mass gravitational-wave signals in ground-based detector data streams, handling data quality is critical to their detection. The low-frequency ranges of ground-based observatories are plagued with non-stationary terrestrial artifacts, called *glitches* [61–63]. Some glitches, similar to signals from high total mass mergers, last for a fraction of a second, making them difficult to distinguish from the signals. These glitches that mimic astrophysical signals can severely decrease the confidence in detection of true gravitational-waves from high total mass mergers [61].

Although a significant fraction of the glitches can be removed by testing them for coherence amongst various ground based detectors and performing matched-filtering, these methods are insufficient to remove all the glitches [61–63]. One method to account for more glitches while searching for high total mass CBC gravitational-

waves is by utilizing a Bayesian odds [64–69]. In this paper, we utilize a Bayesian method, called the Bayesian Coherence Odds-Ratio ρ_{BCR} [66], to rank the candidate gravitational-wave signals from high-mass compact binary coalescences (systems with total masses in the range of 55–500 M_{\odot}) in the detector data recorded during O2. The ρ_{BCR} used in this study is a bootstrap-Bayesian odds computed using Bayesian evidences that describe the explicit probability of data under the hypothesis that the data contains coherent signals vs incoherent glitches, and empirically calculated prior-odds that describe how likely each hypotheses is. [RS: Need to add another couple of sentences describing what is unique about this work. For instance, we study both foreground *and* background events (which is the first time anyone's done a large-scale Bayesian analysis on background data). Suggest using this format: “We highlight a number of innovations unique to this work. First...”] The high-mass candidate ρ_{BCR} values are then used to calculate the probability that the candidate is of astrophysical origins, $p_{\text{astro}}^{\text{BCR}}$. Finally, if the candidate has a p_{astro} reported by the the LIGO-Virgo-KAGRA (LVK) collaboration in GWTC-1 [70], the PyCBC-team [71–80], by the Institute of Advanced study's team (IAS) [81–83], or by Pratten and Vecchio [69], we compare their p_{astro} with the $p_{\text{astro}}^{\text{BCR}}$.

We find that (a) high-mass events reported in the GWTC-1, including GW170729 (the heaviest event in GWTC-1) are very statistically significant $p_{\text{astro}}^{\text{BCR}} > 0.9$; (b) three out of the eight IAS events and candidates have $p_{\text{astro}}^{\text{BCR}} > 0.5$, corroborating IAS's detection claims for those events (GW170304, GW170727, GW170817A), and that (c) our ranking statistic does not identify any new intermediate-mass black holes, but does identify an unreported marginal stellar-mass binary black hole candidate, 170222 with $p_{\text{astro}}^{\text{BCR}} \sim 0.5$.

The remainder of this paper is structured as follows. We outline our methods, including details of our ranking statistic and the retrieval of our candidates in Section II. We present details on the implementation of our analysis in Section III. Finally, we present our results in Section IV, and discuss these results in the context of the significance of gravitational-wave candidates in Section V.

II. METHOD

The standard framework to identify CBC gravitational-wave signals in data is by quantifying the significance of candidates with null-hypothesis significance testing [70, 84]. In this framework, the candidates' ranking statistic is compared against a background distribution in a frequentist approach. The independent matched-filter searches, e.g. PyCBC [76], SPIIR [85] and GstLAL [86], and the coherent burst search cWB [87] used by LVK to search for signals in gravitational-wave data all use ranking statistics in such a manner [70]. Both PyCBC and GstLAL's

ranking statistic incorporate information of the relative likelihood that the data contains a coherent signal versus just noise. In contrast, cWB's ranking statistic uses the information of coherent energy present in the network of detectors [70].

Bayesian inference offers an alternative means to rank the significance of candidate events by computing the odds that the data contain a transient gravitational-wave signal vs. instrumental glitches or noise [66]. This method relies on accurate models for the signal and glitch morphologies and populations [66]. In principle, Bayesian odds is the optimal method for hypothesis testing [67]. Much of its power comes from the Bayesian “evidence”: a marginalized likelihood. The evidence is the correct likelihood of having obtained the data given a hypothesis. However, due to the high computational cost to calculate the evidence, it is not explicitly used in current matched filter searches. Here, we explore a middle-ground hybrid between frequentist matched filtered searches and Bayesian odds. We compute Bayesian evidences for foreground and background data under the assumption that they either contain coherent gravitational-wave signals, noise, or glitches. However, instead of computing true Bayesian odds, we use the evidences to form a bootstrapped distribution for the odds of foreground and background events to form a frequentist ranking statistic.

A. The Bayesian Coherence Odds-Ratio

Bayes theorem states that the posterior probability distribution $p(\vec{\theta}|d, \mathcal{H})$ for data d and a vector of parameters $\vec{\theta}$ that describe a model which quantifies a hypothesis \mathcal{H} , is given by

$$p(\vec{\theta}|d, \mathcal{H}) = \frac{\mathcal{L}(d|\vec{\theta}, \mathcal{H}) \pi(\vec{\theta}|\mathcal{H})}{\mathcal{Z}(d|\mathcal{H})}, \quad (1)$$

where $\mathcal{L}(d|\vec{\theta}, \mathcal{H})$ is the likelihood of the data given the parameters $\vec{\theta}$ and the hypothesis, $\pi(\vec{\theta}|\mathcal{H})$ is the prior probability of the parameters, and finally,

$$\mathcal{Z}(d|\mathcal{H}) = \int_{\vec{\theta}} \mathcal{L}(d|\vec{\theta}, \mathcal{H}) \pi(\vec{\theta}|\mathcal{H}) d\vec{\theta}, \quad (2)$$

is the likelihood after marginalizing over the parameters $\vec{\theta}$. To compare two hypotheses \mathcal{H}_A and \mathcal{H}_B with the Bayes theorem one can calculate an odds-ratio

$$\mathcal{O}_B^A = \frac{\mathcal{Z}^A \pi^A}{\mathcal{Z}^B \pi^B}, \quad (3)$$

where $\{\pi^A, \pi^B\}$ are the prior-odds for each hypothesis and $\{\mathcal{Z}^A, \mathcal{Z}^B\}$ are shorthand for the evidences $\{\mathcal{Z}(d|\mathcal{H}_A), \mathcal{Z}(d|\mathcal{H}_B)\}$. The odds-ratio can quantify which of the two hypotheses is more likely. For example, if

$\mathcal{O}_B^A \gg 1$, then the odds are in favor of the \mathcal{H}_A hypotheses.

The ρ_{BCR} is a Bayesian odds-ratio like the above, of a coherent signal hypotheses \mathcal{H}_S and an incoherent instrumental feature hypothesis \mathcal{H}_I (the null-hypotheses) for a network of D detectors. \mathcal{H}_I states that each detector i has either pure stationary Gaussian noise \mathcal{H}_N or Gaussian noise and an incoherent noise transient (glitch) \mathcal{H}_G . Taking Z^S , Z_i^G and Z_i^N as the Bayesian evidences (defined in Appendix A) for \mathcal{H}_S , \mathcal{H}_N , and \mathcal{H}_G , the ρ_{BCR} is given by

$$\mathcal{O}_{\text{BCR}} = \frac{P^S Z^S}{\prod_{i=1}^D [P^G Z_i^G + (1 - P^G) Z_i^N]}, \quad (4)$$

where P^S and P^G are the prior-odds of obtaining a signal or a glitch from a stretch of data. The prior-odds can be defined more explicitly as

- $P^S = P(\mathcal{H}_S)/P(\mathcal{H}_I)$, the prior-odds for obtaining a coherent signal versus an incoherent instrumental feature.
- $P^G = P(\mathcal{H}_G|\mathcal{H}_I)$, the probability of obtaining a glitch assuming there is an incoherent instrumental feature.

$$\rho_{\text{BCR}} = \frac{\hat{\pi}^S Z^S}{\prod_{i=1}^D [\hat{\pi}^G Z_i^G + (1 - \hat{\pi}^G) Z_i^N]}, \quad (5)$$

[AV: Ranking statistic ρ_{BCR} is like an estimator of what \mathcal{O}_{BCR} is]

When \mathcal{H}_S and \mathcal{H}_I are precisely described and the correct prior-odds are known, the ρ_{BCR} is a Bayesian odds-ratio. As an odds-ratio, the ρ_{BCR} is the optimal discriminator between coherent signals and incoherent instrumental features. However, as the priors-odds are unknown, it is invalid to use the ρ_{BCR} as an odds-ratio to make an informed decision about whether a candidate is from an astrophysical or terrestrial source. Instead of interpreting the ρ_{BCR} as a Bayesian odds-ratio, it can be used as a ranking statistic. Using the ρ_{BCR} as a ranking statistic we can obtain a frequentist significance of a candidate ρ_{BCR} -value measured against a background ρ_{BCR} distribution.

When using the ρ_{BCR} as a detection statistic, the physical interpretation of the prior-odds is lost. Hence, the prior-odds are empirically tuned to maximize the separation between the ρ_{BCR} distribution of the background (expected to favor the \mathcal{H}_I hypothesis) and the ρ_{BCR} distribution of artificially manufactured simulated signals (expected to favor the \mathcal{H}_S hypothesis). Increasing the separation between the two distributions can improve ability of the ρ_{BCR} to discriminate candidate events as coherent signals or incoherent instrumental features. The tuning process is described in detail in Appendix ??.

B. Estimation of astrophysical signal probability

Candidate ρ_{BCR} -values are either statistically insignificant compared to the background ρ_{BCR} distribution, implying the candidate is more probable to be an incoherent instrumental feature (the \mathcal{H}_I null-hypothesis), or statistically significant to the background distribution, indicating the possible presence of an astrophysical signal (the \mathcal{H}_S hypothesis). A false alarm probability with trial factors, FAP, for the candidate ρ_{BCR} -value can quantify the significance. The FAP is the probability that a candidate originating from a non-astrophysical source can be falsely identified as a signal.

To calculate the FAP, each candidate ρ_{BCR} is considered a single statistical trial that can occur at a fixed false alarm probability f , where f is the probability of observing a background ρ_{BCR}' greater than or equal to the candidate ρ_{BCR} ,

$$f = \frac{\text{Count of } \rho_{\text{BCR}}' \leq \rho_{\text{BCR}}}{\text{Count of } \rho_{\text{BCR}}'}. \quad (6)$$

The false alarm probability with trials FAP that the ρ_{BCR} measurement occurs at least once for N trials ($N > 0$), where N is the number of candidate triggers is

$$\text{FAP} = 1 - (1 - f)^N. \quad (7)$$

Finally, the FAP can be used to construct a p_{astro} , the probability that a signal is of astrophysical origin [88–90]

$$p_{\text{astro}} = 1 - \text{FAP}. \quad (8)$$

[AV: Eric, can you take a look at this section about the FAP p-astro?] [AV: The p_{astro} calculation may need some more discussion. Taking $p_{\text{astro}} = 1 - \text{FAP}$ as identifying a real signal can be hugely problematic: https://en.wikipedia.org/wiki/Misuse_of_p-values, even though its ok in this case. Maybe the following papers have something that can help motivate this [91–93]]

C. Data for Analysis

[RS: Rory: Suggest a bit more preamble here, something like “To build a ranking statistic from ρ we need to compute its distribution for foreground and background events. The number of background events in a typical search is very large, however we can manage the number of background triggers by focusing on a specific mass range. Background triggers are generated by search pipelines...]

The LIGO Scientific collaboration operates several search pipelines that scan for gravitational-waves from compact binary mergers such as GstLAL [86], MB-TAOnline [94], SPIIR [85] and PyCBC [76]. The output of PyCBC’s search is a list of times and their corresponding PyCBC ranking statistic ρ_{PC} values. The ρ_{PC}

ranking-statistic is akin to the matched-filter signal-to-noise ratio ρ . However, unlike ρ , ρ_{PC} includes candidate signal's intrinsic and extrinsic properties and other information that feeds into determining if the signal can have astrophysical origins [78]. Whenever a local maximum of $\rho_{\text{PC}} > \rho_{\text{T}}$, where ρ_{T} is some predetermined threshold value, the PyCBC search pipeline produces a single-detector *trigger* associated with the detector and time t_c where the apparent signal in the data has its merger [78].

PyCBC produces three categories of triggers:

- *Candidate event trigger*: a trigger observed with coincident parameters amongst a network of detectors.
- *Simulated trigger*: a trigger detected from an artificially manufactured signal injected into detector data.
- *Background trigger*: a trigger obtained from incoherent signal-free background data (data manufactured by applying relative offsets, or time-slides, between the data of different detectors [78]).

Our work demonstrates that the ρ_{BCR} can be used to measure candidate triggers' statistical significance. The ρ_{BCR} can be a powerful ranking statistic as it incorporates information of not only all possible binary black hole systems that might have merged to produce the trigger but also the various incoherent glitches that might cause a false-detection.

III. ANALYSIS

A. Acquisition of triggers

Advanced LIGO's second observing run O2 lasted 38 weeks [95]. The software package, PyCBC [71], was used by LVK to process the O2 data in 22 time-frames (approximately 2 weeks per frame) and found several gravitational-wave events and numerous gravitational-wave candidates [72–78]. Some candidate events were vetoed to be glitches, while others were rejected due to their low significance. The data are divided into these time-frames because the detector's sensitivity does not stay constant throughout the eight-month-long observing period.

In addition to finding candidate events, PyCBC also identified several million background triggers for each time-frame, by searching background data manufactured by time-sliding data within that time-frame. The background triggers help quantify the candidate events' significance for the respective time-frames. Finally, to test the search's sensitivity, PyCBC produced and searched for thousands of simulated signals.

For our study, we filter the PyCBC background, simulated and candidate triggers to include only high-mass triggers with masses in the ranges of the parameters presented in Table I. A plot of the PyCBC triggers from one

TABLE I. High-mass parameter space (parameters correspond to signals with durations < 454 ms).

	Minimum	Maximum
Component Mass 1 [M_{\odot}]	31.54	491.68
Component Mass 2 [M_{\odot}]	1.32	121.01
Total Mass [M_{\odot}]	56.93	496.72
Chirp Mass [M_{\odot}]	8.00	174.56
Mass Ratio	0.01	0.98

time-frame, during April 23 - May 8, 2017, is presented in Fig. 1. This figure also depicts the gravitational-wave templates used during the search through this time-frame of data.

B. Calculating the BCR for triggers

To evaluate Z^S , Z_i^G and Z_i^N and calculate the ρ_{BCR} Eq. 5 for triggers, we carry out Bayesian inference with BILBY [96, 97], employing DYNESTY [98] as our nested sampler. Nested sampling, an algorithm introduced by Skilling [99, 100], provides an estimate of the Bayesian evidence and is often utilized for parameter estimation within the LIGO collaboration [96, 101, 102].

The most computationally intensive step during Bayesian inference is evaluating the likelihood $\mathcal{L}(d_i|\mu(\vec{\theta}))$. To accelerate our analysis, we use a likelihood that explicitly marginalizes over coalescence time, phase at coalescence, and luminosity distance (Eq. 80 from Thrane and Talbot [103]).

We set the priors $\pi(\vec{\theta}|\mathcal{H}_S)$ and $\pi(\vec{\theta}|\mathcal{H}_G)$ to be identical which reflects our ignorance of the distribution of the population properties of signals and signal-like glitches. These priors restrict signals with mass parameters in the ranges presented in Table I. The spins are aligned over a uniform range for the dimensionless spin magnitude from $[0, 1]$. The luminosity distance prior assigns probability uniformly in comoving volume, with an upper cutoff of 5 Gpc. The full list of the priors, along with their shapes, limits and boundary conditions are documented in Table II.

The waveform template we utilize is IMRPHENOMPv2, a phenomenological waveform template constructed in the frequency domain that models the inspiral, merger, and ring-down (IMR) of a compact binary coalescence [105]. Although there exist gravitational-wave templates such as SEOBNRv4PHM [106] which incorporate more physics, such as information on higher-order modes, we use IMRPHENOMPv2 as it is computationally inexpensive compared to others.

To generate the PSD, we take 31 neighboring off-source non-overlapping 4-second segments of time-series data before the analysis data segment d_i . To suppress spectral leakage, a Tukey window with a 0.2-second roll-off is applied to each data segment. After this the segments are fast-Fourier transformed and median-averaged to create a PSD [107]. Like other PSD estimation methods, this

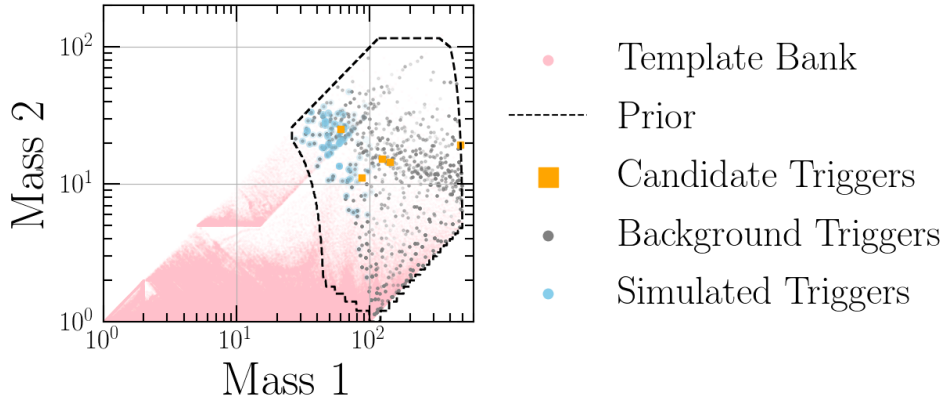


FIG. 1. The template bank (pink) used by PyCBC to search a section of O2 data from April 23 - May 8, 2017. Our search is constrained to the high-mass parameter space enclosed by the dashed line. The candidate, background and simulated triggers detected in this region of the parameter space during this period are plotted in orange, gray and blue respectively.

TABLE II. Prior settings for the parameters used during our parameter estimation. The definitions of the parameters are documented in Romero-Shaw *et al.* [104] Table E1. The trigger time t_c is obtained from the data products of PyCBC’s O2 search.

Parameter	Shape	Limits
\mathcal{M}/M_\odot	Uniform	7–180
q	Uniform	0.1–1
M/M_\odot	Constraint	50–500
d_L/Mpc	Comoving	100–5000
a_1, a_2	Uniform	0–1
θ_{JN}	Sinusoidal	0– π
ψ	Uniform	0– π
ϕ	Uniform	0– 2π
ra	Uniform	0– 2π
dec	Cosine	0– 2π
t_c/s	Uniform	$t_c \pm 0.1$

method adds statistical uncertainties to the PSD [108–110]. To marginalize over the statistical uncertainty, we use the median-likelihood presented by Talbot and Thrane [108] as a post-processing step. We find that this post-processing step improves the search efficiency by 49.26% the details of this calculation are presented in the Appendix C.

Finally, we acquire the foreground, background and data in which we inject simulated signals into, from from the gravitational-wave Open Science Center [95]. The data we use are the publicly accessible O2 strain data from the Hanford and Livingston detectors, recorded while the detectors are in “Science Mode”. We obtain the data using **GWPy** [111].

C. Assigning p_{astro} to candidate events

After the calculating the ρ_{BCR} for the entire set of high-mass background and simulated triggers, we calculate the background and simulated ρ_{BCR} probability distributions for each 2-week time-frame of O2 data. These distributions are used to ‘tune’ prior-odd P^S and P^G values as described in Appendix B.

Using the tuned prior odds the ρ_{BCR} for the candidate events can be calculated. Fig. 2 shows the ρ_{BCR} distributions for the background triggers, simulated triggers and candidate events. The bulk of the background and simulated trigger distributions are separate but slightly overlap due to some of the simulated signal’s being very faint. The separation suggests that the ρ_{BCR} can successfully distinguish signals from noise or glitches. The vertical lines in Fig. 2 displays the ρ_{BCR} for gravitational-wave candidate events. On comparing the candidate event ρ_{BCR} values with the background distribution, we can estimate p_{astro} values for the candidate events.

IV. RESULTS

We analyze the 60,996 background, 5,146 simulated, and 25 candidate triggers reported by PyCBC’s search on the data from LIGO’s second observing run, restricting our analysis to the triggers that fall within our mass-space as described in Section II. We also analyze events and candidate events reported by GWTC-1 and the IAS group (note: some of these were identified as candidates by the PyCBC search). Table III summaries the $p_{\text{astro}}^{\text{BCR}}$, along with the p_{astro} of other pipelines for comparison. Although the various pipeline p_{astro} are not mathematically equivalent, by comparing pipeline p_{astro} values for a given candidate, we can compare how significant each pipeline deems various candidates. The P^S and P^G

TABLE III. The p_{astro} of gravitational wave events from various detection pipelines, along with the event candidates with $p_{\text{astro}}^{\text{BCR}} > 0.3$. Only the candidates and events within our prior space are displayed. The various pipeline p_{astro} represented in this table, $p_{\text{astro}}^{\text{ext}}$, are from the following pipelines: GstLAL \heartsuit [70], PyCBC \clubsuit [70], PyCBC OGC-2 \spadesuit [80], PyCBC ‘single-search’ \diamond [79], IAS \star [82, 83], and Pratten and Vecchio [69]’s significances \blacktriangle . The catalogs labelled IAS-1 and IAS-2 correspond to the candidates published in Venumadhav *et al.* [82] and Zackay *et al.* [83].

Event	Catalog	$p_{\text{astro}}^{\text{BCR}}$	$p_{\text{astro}}^{\text{ext}}$	t_c
GW170104	GWTC-1	0.94	$1.00^{\heartsuit}; 1.00^{\clubsuit}; 1.0^{\blacktriangle}$	1167559934.60
GW170121	IAS-1	0.76	$1.00^{\clubsuit}; 1.00^{\star}; 0.53^{\blacktriangle}$	1169069152.57
170222	-	0.49	-	1171814476.97
170302	IAS-1	0.64	$0.45^{\star}; 0.0^{\blacktriangle}$	1172487815.48
GW170304	IAS-1	0.83	$0.70^{\clubsuit}; 0.99^{\star}; 0.03^{\blacktriangle}$	1172680689.36
GWC170402	IAS-2	0.38	$0.68^{\star}; 0.03^{\diamond}; 0.0^{\blacktriangle}$	1175205126.57
GW170403	IAS-1	0.33	$0.03^{\clubsuit}; 0.56^{\star}; 0.27^{\blacktriangle}$	1175295987.22
GW170425	IAS-1	0.10	$0.21^{\clubsuit}; 0.77^{\star}; 0.74^{\blacktriangle}$	1177134830.18
GW170608	GWTC-1	0.95	$0.92^{\heartsuit}; 1.00^{\clubsuit}; 1.0^{\blacktriangle}$	1180922492.50
GW170727	IAS-1	0.92	$0.99^{\clubsuit}; 0.98^{\star}; 0.66^{\blacktriangle}$	1185152686.02
GW170729	GWTC-1	0.96	$0.98^{\heartsuit}; 0.52^{\clubsuit}; 1.0^{\blacktriangle}$	1185389805.30
GW170809	GWTC-1	0.98	$0.99^{\heartsuit}; 1.00^{\clubsuit}; 1.0^{\blacktriangle}$	1186302517.75
GW170814	GWTC-1	1.00	$1.00^{\heartsuit}; 1.00^{\clubsuit}; 1.0^{\blacktriangle}$	1186741859.53
GW170817A	IAS-2	0.83	$0.86^{\star}; 0.36^{\diamond}; 0.02^{\blacktriangle}$	1186974182.72

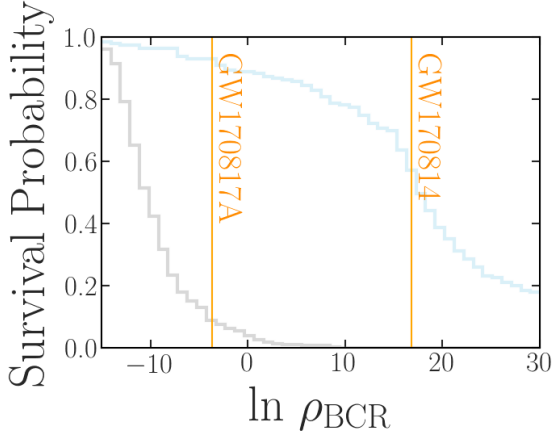


FIG. 2. Histograms represent the survival function (1-CDF) from our high-mass selection of background triggers (gray) and simulated signals (blue) triggers obtained from PyCBC’s search of data from August 13 - 21, 2017. Vertical lines mark the $\ln \rho_{\text{BCR}}$ of IAS’s GW170817A and GWTC-1’s GW170814. [AV: Adjust to have same fonts as other plots]

values utilized for each time-frame are reported in Appendix D.

A. GWTC-1 Events

All the confirmed gravitational-wave events from binary black hole mergers reported in GWTC-1 and within our prior space, (specifically GW170104, GW170608, GW170729, GW170809 and GW170814), have $p_{\text{astro}}^{\text{BCR}} > 0.9$, indicating a high probability of an astrophysical signal.

In addition to the above confirmed gravitational-wave events from GWTC-1, we have also analyzed several candidate events from GWTC-1, most of which have low $p_{\text{astro}}^{\text{BCR}}$. For example, consider the candidate event 170412, assigned a p_{astro} of 0.06 by GstLAL and has a $p_{\text{astro}}^{\text{BCR}}$ of 0.01. This candidate was reported to be excess power caused due noise appearing non-stationary between 60-200 Hz [70]. This candidate acts as an example of how $p_{\text{astro}}^{\text{BCR}}$ may be utilized to eliminate candidates originating from terrestrial noise sources.

B. IAS Events

Our analysis of the high-mass IAS events and candidates in O2 has resulted in three events with disfavored $p_{\text{astro}}^{\text{BCR}} < 0.5$ (GWC170402, GW170403, GW170425), and four events and one candidate with $p_{\text{astro}}^{\text{BCR}} \geq 0.5$ (GW170121, 170302, GW170304, GW170727, GW170817A). While GW170727 and GW170817A’s $p_{\text{astro}}^{\text{BCR}}$ are similar to the p_{astro} reported from IAS (the differences between the p_{astro} from ρ_{BCR} and IAS is

$|\Delta p_{\text{astro}}| < 0.1$), the remaining candidates have opposing p_{astro} values (with $|\Delta p_{\text{astro}}| > 0.15$).

GWC170402, detected by Zackay *et al.* [83], is reported to originate from a binary with non-zero eccentricity [83]. Hence, we might have received a low $p_{\text{astro}}^{\text{BCR}}$ due to our usage of IMRPHENOMPv2, a waveform that does not account for eccentricity. Additionally, the search conducted by Zackay *et al.* [83] was a single-detector search. Our ranking statistic relies on the signal to appear coherent, even if just faintly coherent, amongst the various detectors to have a high $p_{\text{astro}}^{\text{BCR}}$. The lack of coherence and the non-eccentric waveform may be the leading factors for a low p_{astro} . GW170403 and GW170425 which have $p_{\text{astro}}^{\text{BCR}} < 0.35$ also have low p_{astro} reported by Nitz *et al.* [80], suggesting that these events may have been false alarms.

From the candidates with $p_{\text{astro}}^{\text{BCR}} > 0.5$, GW170727 and 170302 are of particular interest, with $p_{\text{astro}}^{\text{BCR}}$ of 0.92 and 0.63. GW170727 was emitted from a black hole binary system with a source frame total mass $\approx 70 M_{\odot}$. In addition to the high $p_{\text{astro}}^{\text{BCR}}$ reported by our study, Venumadhav *et al.* [82] and Nitz *et al.* [80] have also reported high p_{astro} values of 0.98 and 0.99, making it a viable gravitational-wave event candidate. Similarly, the sub-marginal-candidate 170302 reported by [82] with a p_{astro} of 0.45 appears to have a higher significance from our analysis, resulting in a $p_{\text{astro}}^{\text{BCR}}$ of 0.63.

C. New Candidate Events

Although no clear detections are made with the ρ_{BCR} , a marginal-candidate 170222 has been discovered with a $p_{\text{astro}}^{\text{BCR}} \sim 0.5$. This candidate has an $\text{SNR} \sim 7.7$, low spin magnitudes and source-frame component masses of $(47.16^{+8.00}_{-5.77}, 35.50^{+5.79}_{-6.35})M_{\odot}$, making it one of the heavier black-hole mergers from O2 and GWTC-1. This candidate may be of interest as one component black hole may lie in the pair-instability mass gap ($55^{+10}_{-10} - 148^{+13}_{-12}M_{\odot}$) [112, 113]. More details on the candidate are presented in Appendix E. The remaining coherent trigger candidates all have $p_{\text{astro}}^{\text{BCR}} \ll 0.5$ making them unlikely to originate from astrophysical sources.

V. CONCLUSION

Until 2016, a majority of intermediate-mass black hole candidates were from electromagnetic observations. The dawn of gravitational waves astronomy has provided a new lens to identify and study these massive objects – from the mergers of heavy black holes’ gravitational wave emission. In the future, space-based gravitational wave detectors will uncover black holes in the upper end of the intermediate-mass range. In the present, ground-based gravitational-wave observatories can probe the lower-end of the intermediate-mass range. However, many short-duration terrestrial artifacts that mimic intermediate-

mass gravitational-wave signals plague ground-based detectors, making intermediate-mass detection challenging.

In this paper, we demonstrate that the Bayesian Coherence Odds-Ratio ρ_{BCR} [66] can be used as a ranking statistic to provide a measure of significance for gravitational wave signals originating from CBCs with total masses between $55M_{\odot}$ and $400M_{\odot}$, a range that includes intermediate-mass black holes. To compute the ρ_{BCR} for candidates, we utilize Bayesian inference to explicitly calculate the probability of data under various hypotheses (the hypotheses that the data contains a coherent signal, just noise, or an incoherent glitch). This Bayesian ranking method takes a step towards building a unified Bayesian framework that provides a search-pipeline agnostic measure of significance for candidates and estimates their parameters, utilizing the same level of physical information incorporated during detected parameter estimation studies.

In our study, we analyze high-mass candidates detected by PyCBC, the high-mass binary black hole events in O2 reported in GWTC-1 [70] and by the IAS-team [82, 83]. Using $p_{\text{astro}}^{\text{BCR}}$, we find that the high-mass GWTC-1 events have high probabilities of originating from an astrophysical source. We also find that some of the GWTC-1 marginal triggers that have corroborated terrestrial sources (for example, candidate 170412) have low $p_{\text{astro}}^{\text{BCR}}$, indicating this method’s ability to discriminate between terrestrial artifacts and astrophysical signals. Our analysis of the high-mass IAS events demonstrates that GW170121, GW170727, and GW170817A are likely to originate from astrophysical sources, while GWC170402, GW170402, and GW170425 are not. Finally, we do not identify any new gravitational-wave events, but we find a new marginal binary-black hole merger candidate, 170222.

Although our analysis targets high-mass triggers, this method can be extended to include the entire range of LIGO-detectable gravitational-wave sources. Additionally, to further improve the method’s infrastructure, we can use more robust gravitational-wave templates (such as templates that incorporate higher-order modes and orbital precession) and sophisticated glitch models. Future analysis can also incorporate data from all available detectors in a network to increase the sensitivity of $p_{\text{astro}}^{\text{BCR}}$.

ACKNOWLEDGMENTS

The author gratefully thank the PyCBC team for providing the gravitational-wave foreground, background and simulated triggers from PyCBC’s search of O2’s data. We also warmly thank Ian Harry and Thomas Dent for answering questions about the PyCBC search’s data products.

We thank Stuart Anderson for assistance with accommodating this analysis which was performed on the California Institute of Technology computing cluster. All analyses (inclusive of test and failed analyses) performed

for this study used 1.3M core-hours, amounting to a carbon footprint of 167 t of CO² (using the US average electricity source emissions of 0.429 kg/kWh [114] and 0.3 kWh for each CPU).

This research has made use of data, software and/or web tools obtained from the Gravitational Wave Open Science Center (<https://www.gw-openscience.org>), a service of LIGO Laboratory, the LIGO Scientific Collaboration and the Virgo Collaboration. LIGO is funded by the U.S. National Science Foundation. Virgo is funded by the French Centre National de Recherche Scientifique (CNRS), the Italian Istituto Nazionale della Fisica Nucleare (INFN) and the Dutch Nikhef, with contributions by Polish and Hungarian institutes.

Appendix A: Bayesian Evidence Evaluation

1. Noise Model

We assume that each detector’s noise is Gaussian and stationary over the period being analyzed [107]. In practice, we assume that the noise has a mean of zero that the noise variance σ^2 is proportional to the noise power spectral density (PSD) $P(f)$ of the data. Using the $P(f)$, for each frequency-domain data segment d_i in each of the i detectors in a network of D detectors, we can write

$$Z_i^N = \mathcal{N}(d_i | \mu = 0, \sigma^2 = P(f)), \quad (\text{A1})$$

where \mathcal{N} is a normal distribution.

2. Coherent Signal Model

We model coherent signals using a binary black hole waveform template $\mu(\vec{\theta})$, where the vector $\vec{\theta}$ contains a point in the 12 dimensional space describing aligned-spin binary-black hole mergers. For the signal to be coherent, $\vec{\theta}$ must be consistent in each 4-second data segment d_i for a network of D detectors. Hence, the coherent signal evidence is calculated as

$$Z^S = \int \prod_{i=1}^D [\mathcal{L}(d_i | \mu(\vec{\theta}))] \pi(\vec{\theta} | \mathcal{H}_S) d\vec{\theta}, \quad (\text{A2})$$

where $\pi(\vec{\theta} | \mathcal{H}_S)$ is the prior for the parameters in the coherent signal hypothesis, and $\mathcal{L}(d_i | \mu(\vec{\theta}))$ is the likelihood for the coherent signal hypothesis that depends on the gravitational-wave template $\mu(\vec{\theta})$ and its parameters $\vec{\theta}$.

3. Incoherent Glitch Model

Finally, as glitches are challenging to model and poorly understood, we follow Veitch and Vecchio [64] and utilise

a surrogate model for glitches: the glitches are modeled using gravitational-wave templates $\mu(\vec{\theta})$ with uncorrelated parameters amongst the different detectors such that $\vec{\theta}_i \neq \vec{\theta}_j$ for two detectors i and j [64]. Modelling glitches with $\mu(\vec{\theta})$ captures the worst case scenario: when glitches are identical to gravitational-wave signals (excluding coherent signals). Thus, we can write Z_i^G as

$$Z_i^G = \int_{\vec{\theta}} \mathcal{L}(d_i | \mu(\vec{\theta})) \pi(\vec{\theta} | \mathcal{H}_G) d\vec{\theta}, \quad (\text{A3})$$

where $\pi(\vec{\theta} | \mathcal{H}_G)$ is the prior for the parameters in the incoherent glitch hypothesis.

Appendix B: Tuning the prior-odds

After calculating the ρ_{BCR} for a set of background triggers and simulated triggers from a stretch of detector-data (a data chunk), we can compute probability distributions for the background and simulated triggers, $p_b(\rho_{\text{BCR}})$ and $p_s(\rho_{\text{BCR}})$. We expect the background trigger and simulated signal ρ_{BCR} values to favor the incoherent glitch and the coherent signal hypothesis, respectively. Ideally, these distributions representing two unique populations should be distinctly separate and have no overlap in their ρ_{BCR} values. The prior odds parameters P^S and P^G from Eq. 5 help separate the two distributions. Altering P^S translates the ρ_{BCR} probability distributions while adjusting P^G spreads the distributions. Although Bayesian hyper-parameter estimation can determine the optimal values for P^S and P^G , an easier approach is to adjust the parameters for each data chunk’s ρ_{BCR} distribution. In this study, we tune P^S and P^G to maximally separate the ρ_{BCR} distributions for the background and simulated triggers.

To calculate the separation between $p_b(\rho_{\text{BCR}})$ and $p_s(\rho_{\text{BCR}})$, we use the Kullback–Leibler divergence (KL divergence) D_{KL} , given by

$$D_{KL}(p_b | p_s) = \sum_{x \in \rho_{\text{BCR}}} p_b(x) \log \left(\frac{p_b(x)}{p_s(x)} \right). \quad (\text{B1})$$

The $D_{KL} = 0$ when the distributions are identical and increases as the asymmetry between the distributions increases.

We limit our search for the maximum KL-divergence in the P^S and P^G ranges of $[10^{-10}, 10^0]$. We set our values for P^S and P^G to those which provide the highest KL-divergence and calculate the ρ_{BCR} for candidate events present in this data chunk. Note that we conduct the analysis in data chunks of a few days rather than an entire data set of a few months as the background may be different at different points of the entire data set.

Appendix C: Marginalizing over PSD statistical uncertainties

To generate the results in Fig. 2, we applied a post-processing step to marginalize the uncertainty in the PSD. In Fig. 3, we show the results if this post-processing step is not applied. Clearly, marginalizing over uncertainty in the PSD yields an improvement in the separation of the noise and signal distributions. Quantitatively, at a threshold $\rho_{\text{BCR}}^T = 0$ the post-processing step results in a reduction in the number of background $\rho_{\text{BCR}} > \rho_{\text{BCR}}^T$ from 60.7% to 25.28% in the August 13 - 21, 2017 time-frame of data. For the entirety of O2 PSD marginalization resulted in a 49.26% improvement in search efficiency.

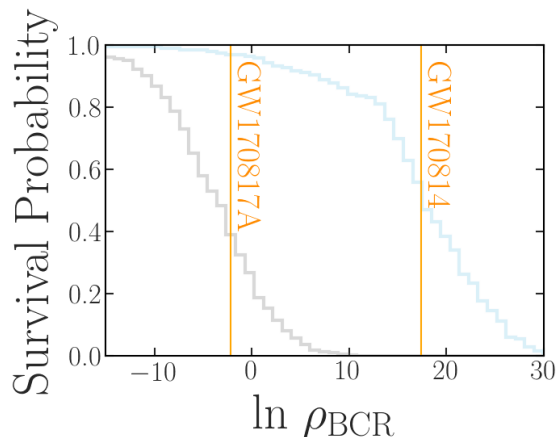


FIG. 3. This plot is analogous to Fig. 2, but without using the post-processing step to marginalize over PSD statistical uncertainties. Without the post-processing step, there is a greater overlap between the background (gray) and foreground (blue) survival functions. For more details about this plot, refer to the caption of Fig. 2.

Appendix D: Tuned prior odds

O2 lasted several months over which the detector's sensitivity varied. Hence, a part of our analysis entailed tuning the prior odds for obtaining a signal and a glitch, P^S and P^G , as described in Section II. Table IV presents the signal and glitch prior odds utilized for each time-frame of O2 data.

Tuning the prior odds can dramatically affect the

$p_{\text{astro}}^{\text{BCR}}$. For example, consider Table V, which reports tuned $p_{\text{astro}}^{\text{BCR}}$ and un-tuned $p_{\text{astro}}^{\text{BCR}'}$ (where $P^S = 1$ and $P^G = 1$) for various high-mass events and candidates. By tuning the prior odds, the $p_{\text{astro}}^{\text{BCR}}$ for some IAS events (for example, GW170403 and GW170817A) can change by more than 0.5, resulting in the promotion/demotion of a candidate's significance.

TABLE IV. The prior odds used for each time-frame of data from O2. Each time frame commences at the start date and concludes at the following time-frame's start date.

Start Date	$\hat{\pi}^S$	$\hat{\pi}^G$
2016-11-15	-	-
2016-11-30	-	-
2016-12-23	1.00E+00	6.25E-01
2017-01-22	1.00E+00	2.33E-02
2017-02-03	1.00E-10	2.44E-01
2017-02-12	1.76E-08	5.96E-02
2017-02-20	6.55E-10	2.22E-03
2017-02-28	1.00E-10	5.96E-02
2017-03-10	2.56E-10	3.91E-01
2017-03-18	1.60E-10	1.00E+00
2017-03-27	1.10E-08	5.96E-02
2017-04-04	3.73E-02	2.33E-02
2017-04-14	1.05E-09	2.44E-01
2017-04-23	2.68E-09	1.46E-02
2017-05-08	1.00E+00	2.44E-01
2017-06-18	6.55E-10	3.39E-04
2017-06-30	2.02E-05	5.69E-03
2017-07-15	1.05E-09	9.54E-02
2017-07-27	1.00E+00	2.12E-04
2017-08-05	2.12E-04	3.73E-02
2017-08-13	2.68E-09	8.69E-04
2017-08-21	-	-

Appendix E: A closer look at 170222

PyCBC found the candidate 170222 with $\mathcal{M}_c = 49.46$ and $q = 0.68$, values that fall within our uncertainty limits. Some of the posteriors that were produced as a by-product of our ρ_{BCR} calculation can be viewed in Fig. 4.

[1] B. L. Webster and P. Murdin, Cygnus X-1-a Spectroscopic Binary with a Heavy Companion ?, *Nature* **235**, 37 (1972).

[2] B. Balick and R. L. Brown, Intense sub-arcsecond structure in the galactic center., *ApJ* **194**, 265 (1974).

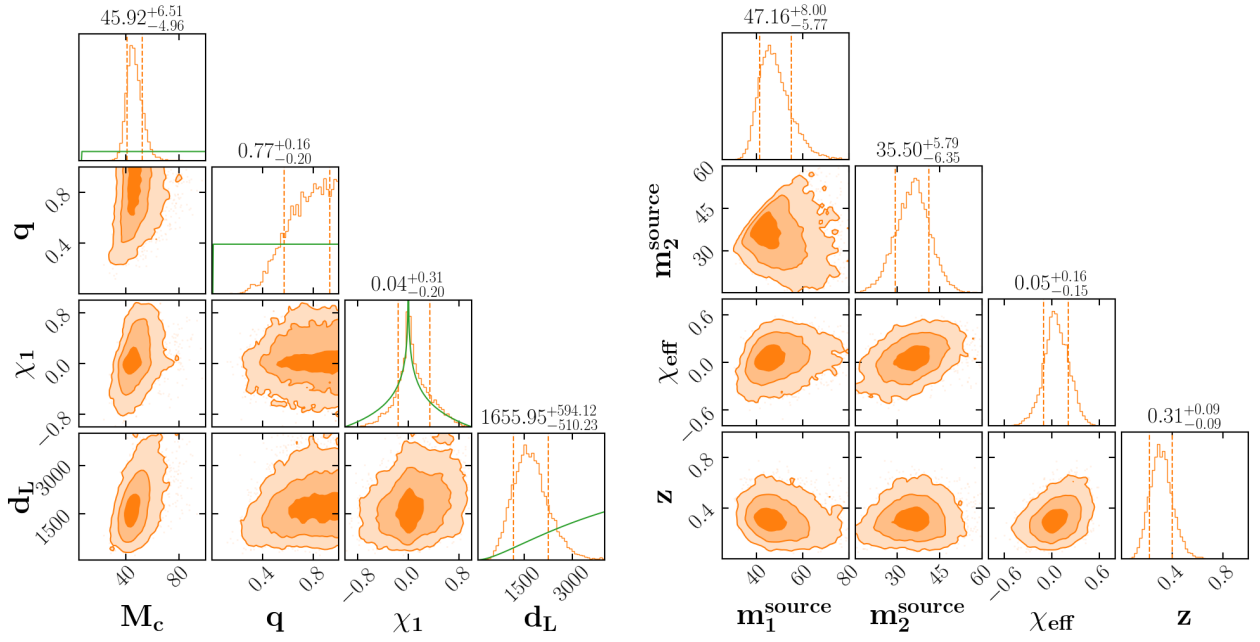


FIG. 4. Posterior distributions for some parameters of 170222, comparing posteriors in orange and prior probability density functions to the one-dimensional marginal distributions in green. Left: Posterior probability distributions for 4 of the 11 search parameters. Sections of the prior probability density functions used for analysis are displayed in green in one-dimensional marginal distributions plots. Right: Posterior probability distributions for some inferred parameters. [AV: Right plot labels being cut off. Should i plot prior-samples on the right?]

TABLE V. The BCR p-astro after tuning the prior odds, $p_{\text{astro}}^{\text{BCR}}$, and without tuning the prior odds, $p_{\text{astro}}^{\text{BCR}'}$ (where $P^S = 1$ and $P^G = 1$).

Event	Catalog	$p_{\text{astro}}^{\text{BCR}}$	$p_{\text{astro}}^{\text{BCR}'}$
161202	-	0.09	0.41
GW170104	GWTC-1	0.94	0.93
GW170121	IAS-1	0.76	0.72
170206	-	0.11	0.52
170222	-	0.49	0.49
170302	IAS-1	0.64	0.54
GW170304	IAS-1	0.83	0.81
GWC170402	IAS-2	0.38	0.01
GW170403	IAS-1	0.33	0.89
GW170425	IAS-1	0.10	0.22
GW170608	GWTC-1	0.95	0.95
GW170727	IAS-1	0.92	0.96
GW170729	GWTC-1	0.96	0.94
GW170809	GWTC-1	0.98	0.99
GW170814	GWTC-1	1.00	1.00
GW170817A	IAS-2	0.83	0.36

- [3] A. M. Ghez, B. L. Klein, M. Morris, and E. E. Becklin, High Proper-Motion Stars in the Vicinity of Sagittarius A*: Evidence for a Supermassive Black Hole at the Center of Our Galaxy, *ApJ* **509**, 678 (1998), arXiv:astro-ph/9807210 [astro-ph].
- [4] R. Genzel, F. Eisenhauer, and S. Gillessen, The Galactic Center massive black hole and nuclear star cluster, *Reviews of Modern Physics* **82**, 3121 (2010), arXiv:1006.0064 [astro-ph.GA].
- [5] B. P. Abbott, R. Abbott, T. D. Abbott, S. Abraham, and et al., GWTC-1: A Gravitational-Wave Transient Catalog of Compact Binary Mergers Observed by LIGO and Virgo during the First and Second Observing Runs, *Physical Review X* **9**, 031040 (2019), arXiv:1811.12907 [astro-ph.HE].
- [6] Event Horizon Telescope Collaboration, K. Akiyama, A. Alberdi, W. Alef, and et al., First M87 Event Horizon Telescope Results. I. The Shadow of the Supermassive Black Hole, *ApJ* **875**, L1 (2019), arXiv:1906.11238 [astro-ph.GA].
- [7] R. Abbott, T. D. Abbott, S. Abraham, F. Acernese, and et al., GWTC-2: Compact Binary Coalescences Observed by LIGO and Virgo During the First Half of the Third Observing Run, arXiv e-prints, arXiv:2010.14527 (2020), arXiv:2010.14527 [gr-qc].
- [8] H. Tagawa, B. Kocsis, Z. Haiman, I. Bartos, K. Omukai, and J. Samsing, Mass-gap Mergers in Active Galactic Nuclei, *ApJ* **908**, 194 (2021), arXiv:2012.00011 [astro-ph.HE].
- [9] Y.-P. Li, A. M. Dempsey, S. Li, H. Li, and J. Li, Orbital evolution of binary black holes in active galactic nucleus disks: a disk channel for binary black

- hole mergers?, arXiv e-prints , arXiv:2101.09406 (2021), arXiv:2101.09406 [astro-ph.HE].
- [10] J. Samsing, I. Bartos, D. J. D’Orazio, Z. Haiman, B. Kocsis, N. W. C. Leigh, B. Liu, M. E. Pesah, and H. Tagawa, Active Galactic Nuclei as Factories for Eccentric Black Hole Mergers, arXiv e-prints , arXiv:2010.09765 (2020), arXiv:2010.09765 [astro-ph.HE].
 - [11] H. Tagawa, Z. Haiman, and B. Kocsis, Formation and Evolution of Compact-object Binaries in AGN Disks, *ApJ* **898**, 25 (2020), arXiv:1912.08218 [astro-ph.GA].
 - [12] W. Ishibashi and M. Gröbner, Evolution of binary black holes in AGN accretion discs: Disc-binary interaction and gravitational wave emission, *A&A* **639**, A108 (2020), arXiv:2006.07407 [astro-ph.GA].
 - [13] M. Gröbner, W. Ishibashi, S. Tiwari, M. Haney, and P. Jetzer, Binary black hole mergers in AGN accretion discs: gravitational wave rate density estimates, *A&A* **638**, A119 (2020), arXiv:2005.03571 [astro-ph.GA].
 - [14] Y. Yang, I. Bartos, V. Gayathri, K. E. S. Ford, and et al., Hierarchical Black Hole Mergers in Active Galactic Nuclei, *Phys. Rev. Lett.* **123**, 181101 (2019), arXiv:1906.09281 [astro-ph.HE].
 - [15] B. McKernan, K. E. S. Ford, I. Bartos, M. J. Graham, W. Lyra, S. Marka, Z. Marka, N. P. Ross, D. Stern, and Y. Yang, Ram-pressure Stripping of a Kicked Hill Sphere: Prompt Electromagnetic Emission from the Merger of Stellar Mass Black Holes in an AGN Accretion Disk, *ApJ* **884**, L50 (2019), arXiv:1907.03746 [astro-ph.HE].
 - [16] Y. Yang, I. Bartos, Z. Haiman, B. Kocsis, Z. Márka, N. C. Stone, and S. Márka, AGN Disks Harden the Mass Distribution of Stellar-mass Binary Black Hole Mergers, *ApJ* **876**, 122 (2019), arXiv:1903.01405 [astro-ph.HE].
 - [17] B. McKernan, K. E. S. Ford, J. Bellovary, N. W. C. Leigh, and et al., Constraining Stellar-mass Black Hole Mergers in AGN Disks Detectable with LIGO, *ApJ* **866**, 66 (2018), arXiv:1702.07818 [astro-ph.HE].
 - [18] J. M. Bellovary, M.-M. Mac Low, B. McKernan, and K. E. S. Ford, Migration Traps in Disks around Supermassive Black Holes, *ApJ* **819**, L17 (2016), arXiv:1511.00005 [astro-ph.GA].
 - [19] B. McKernan, K. E. S. Ford, B. Kocsis, W. Lyra, and L. M. Winter, Intermediate-mass black holes in AGN discs - II. Model predictions and observational constraints, *MNRAS* **441**, 900 (2014), arXiv:1403.6433 [astro-ph.GA].
 - [20] B. McKernan, K. E. S. Ford, W. Lyra, and H. B. Perets, Intermediate mass black holes in AGN discs - I. Production and growth, *MNRAS* **425**, 460 (2012), arXiv:1206.2309 [astro-ph.GA].
 - [21] S. Banerjee, Stellar-mass black holes in young massive and open stellar clusters - V. comparisons with LIGO-Virgo merger rate densities, *MNRAS* **503**, 3371 (2021), arXiv:2011.07000 [astro-ph.HE].
 - [22] M. Zevin, S. S. Bavera, C. P. L. Berry, V. Kalogera, T. Fragos, P. Marchant, C. L. Rodriguez, F. Antonini, D. E. Holz, and C. Pankow, One Channel to Rule Them All? Constraining the Origins of Binary Black Holes Using Multiple Formation Pathways, *ApJ* **910**, 152 (2021), arXiv:2011.10057 [astro-ph.HE].
 - [23] M. Mapelli, M. Dall’Amico, Y. Bouffanais, N. Giacobbo, and et al., Hierarchical black hole mergers in young, globular and nuclear star clusters: the effect of metallicity, spin and cluster properties, arXiv e-prints , arXiv:2103.05016 (2021), arXiv:2103.05016 [astro-ph.HE].
 - [24] N. C. Weatherford, G. Fragione, K. Kremer, S. Chatterjee, C. S. Ye, C. L. Rodriguez, and F. A. Rasio, Black Hole Mergers from Star Clusters with Top-heavy Initial Mass Functions, *ApJ* **907**, L25 (2021), arXiv:2101.02217 [astro-ph.GA].
 - [25] Y. Bouffanais, M. Mapelli, F. Santoliquido, N. Giacobbo, U. N. Di Carlo, S. Rastello, M. C. Artale, and G. Iorio, New insights on binary black hole formation channels after GWTC-2: young star clusters versus isolated binaries, arXiv e-prints , arXiv:2102.12495 (2021), arXiv:2102.12495 [astro-ph.HE].
 - [26] A. Ballone, S. Torniamenti, M. Mapelli, U. N. Di Carlo, M. Spera, S. Rastello, N. Gaspari, and G. Iorio, From hydrodynamics to N-body simulations of star clusters: mergers and rotation, *MNRAS* **501**, 2920 (2021), arXiv:2012.00767 [astro-ph.GA].
 - [27] J. Kumamoto, M. S. Fujii, A. A. Trani, and A. Tanikawa, Spin distribution of binary black holes formed in open clusters, arXiv e-prints , arXiv:2102.09323 (2021), arXiv:2102.09323 [astro-ph.HE].
 - [28] S. Banerjee, Stellar-mass black holes in young massive and open stellar clusters - IV. Updated stellar-evolutionary and black hole spin models and comparisons with the LIGO-Virgo O1/O2 merger-event data, *MNRAS* **500**, 3002 (2021), arXiv:2004.07382 [astro-ph.HE].
 - [29] M. A. S. Martinez, G. Fragione, K. Kremer, S. Chatterjee, and et al., Black Hole Mergers from Hierarchical Triples in Dense Star Clusters, *ApJ* **903**, 67 (2020), arXiv:2009.08468 [astro-ph.GA].
 - [30] I. Romero-Shaw, P. D. Lasky, E. Thrane, and J. Calderón Bustillo, GW190521: Orbital Eccentricity and Signatures of Dynamical Formation in a Binary Black Hole Merger Signal, *ApJ* **903**, L5 (2020), arXiv:2009.04771 [astro-ph.HE].
 - [31] O. Agnastou, M. Trenti, and A. Melatos, Dynamically formed black hole binaries: In-cluster versus ejected mergers, *PASA* **37**, e044 (2020), arXiv:2009.00178 [astro-ph.HE].
 - [32] A. Toubiana, L. Sberna, A. Caputo, G. Cusin, and et al., Detectable Environmental Effects in GW190521-like Black-Hole Binaries with LISA, *Phys. Rev. Lett.* **126**, 101105 (2021), arXiv:2010.06056 [astro-ph.HE].
 - [33] E. Farrell, J. H. Groh, R. Hirschi, L. Murphy, E. Kaiser, S. Ekström, C. Georgy, and G. Meynet, Is GW190521 the merger of black holes from the first stellar generations?, *MNRAS* **502**, L40 (2021), arXiv:2009.06585 [astro-ph.SR].
 - [34] M. Safarzadeh and Z. Haiman, Formation of GW190521 via Gas Accretion onto Population III Stellar Black Hole Remnants Born in High-redshift Minihalos, *ApJ* **903**, L21 (2020), arXiv:2009.09320 [astro-ph.HE].
 - [35] B. Liu and V. Bromm, Gravitational waves from Population III binary black holes formed by dynamical capture, *MNRAS* **495**, 2475 (2020), arXiv:2003.00065 [astro-ph.CO].
 - [36] K. Inayoshi, R. Hirai, T. Kinugawa, and K. Hotokezaka, Formation pathway of Population III coalescing binary black holes through stable mass transfer, *MNRAS* **468**, 5020 (2017), arXiv:1701.04823 [astro-ph.HE].

- [37] A. Askar, M. B. Davies, and R. P. Church, Formation of supermassive black holes in galactic nuclei - I. Delivering seed intermediate-mass black holes in massive stellar clusters, *MNRAS* **502**, 2682 (2021), arXiv:2006.04922 [astro-ph.GA].
- [38] M. Arca Sedda and A. Mastrobuono-Battisti, Mergers of globular clusters in the Galactic disc: intermediate mass black hole coalescence and implications for gravitational waves detection, arXiv e-prints, arXiv:1906.05864 (2019), arXiv:1906.05864 [astro-ph.GA].
- [39] P. Amaro-Seoane, J. R. Gair, M. Freitag, M. C. Miller, I. Mandel, C. J. Cutler, and S. Babak, TOPICAL REVIEW: Intermediate and extreme mass-ratio inspirals—astrophysics, science applications and detection using LISA, *Classical and Quantum Gravity* **24**, R113 (2007), arXiv:astro-ph/0703495 [astro-ph].
- [40] M. A. Gürkan, J. M. Fregeau, and F. A. Rasio, Massive Black Hole Binaries from Collisional Runaways, *ApJ* **640**, L39 (2006), arXiv:astro-ph/0512642 [astro-ph].
- [41] B. M. Peterson, Measuring the Masses of Supermassive Black Holes, *Space Sci. Rev.* **183**, 253 (2014).
- [42] R. Schödel, T. Ott, R. Genzel, R. Hofmann, and et al., A star in a 15.2-year orbit around the supermassive black hole at the centre of the Milky Way, *Nature* **419**, 694 (2002), arXiv:astro-ph/0210426 [astro-ph].
- [43] B. Kiziltan, H. Baumgardt, and A. Loeb, An intermediate-mass black hole in the centre of the globular cluster 47 Tucanae, *Nature* **542**, 203 (2017), arXiv:1702.02149 [astro-ph.GA].
- [44] A. W. Graham and N. Scott, The $M_{BH-L_{spheroid}}$ Relation at High and Low Masses, the Quadratic Growth of Black Holes, and Intermediate-mass Black Hole Candidates, *ApJ* **764**, 151 (2013), arXiv:1211.3199 [astro-ph.CO].
- [45] T. Wevers, S. van Velzen, P. G. Jonker, N. C. Stone, T. Hung, F. Onori, S. Gezari, and N. Blagorodnova, Black hole masses of tidal disruption event host galaxies, *MNRAS* **471**, 1694 (2017), arXiv:1706.08965 [astro-ph.GA].
- [46] J. E. Greene and L. C. Ho, Active Galactic Nuclei with Candidate Intermediate-Mass Black Holes, *ApJ* **610**, 722 (2004), arXiv:astro-ph/0404110 [astro-ph].
- [47] D. Lin, J. Strader, A. J. Romanowsky, J. A. Irwin, O. Godet, D. Barret, N. A. Webb, J. Homan, and R. A. Remillard, Multiwavelength Follow-up of the Hyperluminous Intermediate-mass Black Hole Candidate 3XMM J215022.4-055108, *ApJ* **892**, L25 (2020), arXiv:2002.04618 [astro-ph.HE].
- [48] J. Paynter, R. Webster, and E. Thrane, Evidence for an intermediate-mass black hole from a gravitationally lensed gamma-ray burst, *Nature Astronomy* 10.1038/s41550-021-01307-1 (2021).
- [49] J. E. Greene, J. Strader, and L. C. Ho, Intermediate-Mass Black Holes, *ARA&A* **58**, 257 (2020), 2021 review on IMBH, arXiv:1911.09678 [astro-ph.GA].
- [50] F. Koliopanos, Intermediate Mass Black Holes: A Review, in *XII Multifrequency Behaviour of High Energy Cosmic Sources Workshop (MULTIF2017)* (2017) p. 51, arXiv:1801.01095 [astro-ph.GA].
- [51] M. Mezcuca, Observational evidence for intermediate-mass black holes, *International Journal of Modern Physics D* **26**, 1730021 (2017), arXiv:1705.09667 [astro-ph.GA].
- [52] A. Ridolfi, P. C. C. Freire, P. Torne, C. O. Heinke, and et al., Long-term observations of the pulsars in 47 Tucanae - I. A study of four elusive binary systems, *MNRAS* **462**, 2918 (2016), arXiv:1607.07248 [astro-ph.HE].
- [53] P. C. C. Freire, A. Ridolfi, M. Kramer, C. Jordan, and et al., Long-term observations of the pulsars in 47 Tucanae - II. Proper motions, accelerations and jerks, *MNRAS* **471**, 857 (2017), arXiv:1706.04908 [astro-ph.HE].
- [54] G. L. Israel, A. Papitto, P. Esposito, L. Stella, and et al., Discovery of a 0.42-s pulsar in the ultraluminous X-ray source NGC 7793 P13, *MNRAS* **466**, L48 (2017), arXiv:1609.06538 [astro-ph.HE].
- [55] G. A. Rodríguez Castillo, G. L. Israel, A. Belfiore, F. Bernardini, and et al., Discovery of a 2.8 s Pulsar in a 2 Day Orbit High-mass X-Ray Binary Powering the Ultraluminous X-Ray Source ULX-7 in M51, *ApJ* **895**, 60 (2020), arXiv:1906.04791 [astro-ph.HE].
- [56] R. Abbott, T. D. Abbott, S. Abraham, F. Acernese, and et al., GW190521: A Binary Black Hole Merger with a Total Mass of 150 M_{\odot} , *Phys. Rev. Lett.* **125**, 101102 (2020), arXiv:2009.01075 [gr-qc].
- [57] LIGO Scientific Collaboration, J. Aasi, B. P. Abbott, R. Abbott, and et al., Advanced LIGO, *Classical and Quantum Gravity* **32**, 074001 (2015), arXiv:1411.4547 [gr-qc].
- [58] D. V. Martynov, E. D. Hall, B. P. Abbott, R. Abbott, and et al., Sensitivity of the Advanced LIGO detectors at the beginning of gravitational wave astronomy, *Phys. Rev. D* **93**, 112004 (2016), arXiv:1604.00439 [astro-ph.IM].
- [59] C. J. Moore, R. H. Cole, and C. P. L. Berry, Gravitational-wave sensitivity curves, *Classical and Quantum Gravity* **32**, 015014 (2014).
- [60] X.-Y. Lu, Y.-J. Tan, and C.-G. Shao, Sensitivity functions for space-borne gravitational wave detectors, *Phys. Rev. D* **100**, 044042 (2019), arXiv:2007.03400 [gr-qc].
- [61] A. H. Nitz, Distinguishing short duration noise transients in LIGO data to improve the PyCBC search for gravitational waves from high mass binary black hole mergers, *Classical and Quantum Gravity* **35**, 035016 (2018), arXiv:1709.08974 [gr-qc].
- [62] J. Powell, Parameter estimation and model selection of gravitational wave signals contaminated by transient detector noise glitches, *Classical and Quantum Gravity* **35**, 155017 (2018), arXiv:1803.11346 [astro-ph.IM].
- [63] M. Cabero, A. Lundgren, A. H. Nitz, T. Dent, D. Barker, E. Goetz, J. S. Kissel, L. K. Nuttall, P. Schale, R. Schofield, and D. Davis, Blip glitches in Advanced LIGO data, *Classical and Quantum Gravity* **36**, 155010 (2019), arXiv:1901.05093 [physics.ins-det].
- [64] J. Veitch and A. Vecchio, Bayesian coherent analysis of in-spiral gravitational wave signals with a detector network, *Phys. Rev. D* **81**, 062003 (2010), arXiv:0911.3820 [astro-ph.CO].
- [65] J. B. Kanner, T. B. Littenberg, N. Cornish, M. Millhouse, E. Xhakaj, F. Salemi, M. Drago, G. Vedovato, and S. Klimenko, Leveraging waveform complexity for confident detection of gravitational waves, *Physical Review D* **93**, 022002 (2016).
- [66] M. Isi, R. Smith, S. Vitale, T. J. Massinger, J. Kanner, and A. Vajpeyi, Enhancing confidence in the detection of gravitational waves from compact binaries using signal coherence, *Phys. Rev. D* **98**, 042007 (2018),

- arXiv:1803.09783 [gr-qc].
- [67] G. Ashton, E. Thrane, and R. J. E. Smith, Gravitational wave detection without boot straps: A Bayesian approach, *Phys. Rev. D* **100**, 123018 (2019), arXiv:1909.11872 [gr-qc].
 - [68] G. Ashton and E. Thrane, The astrophysical odds of GW151216, *MNRAS* **10.1093/mnras/staa2332** (2020), arXiv:2006.05039 [astro-ph.HE].
 - [69] G. Pratten and A. Vecchio, Assessing gravitational-wave binary black hole candidates with Bayesian odds, arXiv e-prints, arXiv:2008.00509 (2020), arXiv:2008.00509 [gr-qc].
 - [70] B. P. Abbott, R. Abbott, T. D. Abbott, *et al.* (LIGO Scientific Collaboration and Virgo Collaboration), GWTC-1: A Gravitational-Wave Transient Catalog of Compact Binary Mergers Observed by LIGO and Virgo during the First and Second Observing Runs, *Phys. Rev. X* **9**, 031040 (2019).
 - [71] A. Nitz, I. Harry, D. Brown, C. M. Biwer, J. Willis, T. D. Canton, C. Capano, L. Pekowsky, T. Dent, A. R. Williamson, G. S. Davies, S. De, M. Cabero, B. Machenschalk, P. Kumar, S. Reyes, D. Macleod, F. Pannarale, dfinstad, T. Massinger, M. Tápai, L. Singer, S. Khan, S. Fairhurst, S. Kumar, A. Nielsen, shasvath, I. Dorrington, A. Lenon, and H. Gabbard, gwastro/pycbc: PyCBC Release 1.16.4 (2020).
 - [72] B. Allen, W. G. Anderson, P. R. Brady, D. A. Brown, and J. D. E. Creighton, FINDCHIRP: An algorithm for detection of gravitational waves from inspiraling compact binaries, *Phys. Rev. D* **85**, 122006 (2012), arXiv:gr-qc/0509116 [gr-qc].
 - [73] B. Allen, χ^2 time-frequency discriminator for gravitational wave detection, *Phys. Rev. D* **71**, 062001 (2005), arXiv:gr-qc/0405045 [gr-qc].
 - [74] A. H. Nitz, T. Dent, T. Dal Canton, S. Fairhurst, and D. A. Brown, Detecting Binary Compact-object Mergers with Gravitational Waves: Understanding and Improving the Sensitivity of the PyCBC Search, *ApJ* **849**, 118 (2017), arXiv:1705.01513 [gr-qc].
 - [75] T. Dal Canton, A. H. Nitz, A. P. Lundgren, A. B. Nielsen, D. A. Brown, T. Dent, I. W. Harry, B. Krishnan, A. J. Miller, K. Wette, K. Wiesner, and J. L. Willis, Implementing a search for aligned-spin neutron star-black hole systems with advanced ground based gravitational wave detectors, *Phys. Rev. D* **90**, 082004 (2014), arXiv:1405.6731 [gr-qc].
 - [76] S. A. Usman, A. H. Nitz, I. W. Harry, C. M. Biwer, D. A. Brown, M. Cabero, C. D. Capano, T. Dal Canton, T. Dent, S. Fairhurst, M. S. Kehl, D. Keppel, B. Krishnan, A. Lenon, A. Lundgren, A. B. Nielsen, L. P. Pekowsky, H. P. Pfeiffer, P. R. Saulson, M. West, and J. L. Willis, The PyCBC search for gravitational waves from compact binary coalescence, *Classical and Quantum Gravity* **33**, 215004 (2016), arXiv:1508.02357 [gr-qc].
 - [77] A. H. Nitz, T. Dal Canton, D. Davis, and S. Reyes, Rapid detection of gravitational waves from compact binary mergers with PyCBC Live, *Phys. Rev. D* **98**, 024050 (2018), arXiv:1805.11174 [gr-qc].
 - [78] G. S. Davies, T. Dent, M. Tápai, I. Harry, C. McIsaac, and A. H. Nitz, Extending the PyCBC search for gravitational waves from compact binary mergers to a global network, *Phys. Rev. D* **102**, 022004 (2020), arXiv:2002.08291 [astro-ph.HE].
 - [79] A. H. Nitz, T. Dent, G. S. Davies, and I. Harry, A Search for Gravitational Waves from Binary Mergers with a Single Observatory, *ApJ* **897**, 169 (2020), arXiv:2004.10015 [astro-ph.HE].
 - [80] A. H. Nitz, T. Dent, G. S. Davies, S. Kumar, C. D. Capano, I. Harry, S. Mozzon, L. Nuttall, A. Lundgren, and M. Tápai, 2-OGC: Open Gravitational-wave Catalog of Binary Mergers from Analysis of Public Advanced LIGO and Virgo Data, *ApJ* **891**, 123 (2020), arXiv:1910.05331 [astro-ph.HE].
 - [81] T. Venumadhav, B. Zackay, J. Roulet, L. Dai, and M. Zaldarriaga, New search pipeline for compact binary mergers: Results for binary black holes in the first observing run of Advanced LIGO, *Physical Review D* **100**, 023011 (2019).
 - [82] T. Venumadhav, B. Zackay, J. Roulet, L. Dai, and M. Zaldarriaga, New Binary Black Hole Mergers in the Second Observing Run of Advanced LIGO and Advanced Virgo, arXiv e-prints, arXiv:1904.07214 (2019), arXiv:1904.07214 [astro-ph.HE].
 - [83] B. Zackay, L. Dai, T. Venumadhav, J. Roulet, and M. Zaldarriaga, Detecting Gravitational Waves With Disparate Detector Responses: Two New Binary Black Hole Mergers, arXiv e-prints, arXiv:1910.09528 (2019), arXiv:1910.09528 [astro-ph.HE].
 - [84] B. P. Abbott, R. Abbott, T. D. Abbott, *et al.*, GWTC-2: Compact Binary Coalescences Observed by LIGO and Virgo During the First Half of the Third Observing Run, arXiv e-prints, arXiv:2010.14527 (2020), arXiv:2010.14527 [gr-qc].
 - [85] Q. Chu, M. Kovalam, L. Wen, T. Slaven-Blair, and *et al.*, The SPIIR online coherent pipeline to search for gravitational waves from compact binary coalescences, arXiv e-prints, arXiv:2011.06787 (2020), arXiv:2011.06787 [gr-qc].
 - [86] S. Sachdev, S. Caudill, H. Fong, R. K. Lo, C. Messick, D. Mukherjee, R. Magee, L. Tsukada, K. Blackburn, P. Brady, *et al.*, The GstLAL Search Analysis Methods for Compact Binary Mergers in Advanced LIGO's Second and Advanced Virgo's First Observing Runs, arXiv preprint arXiv:1901.08580 (2019).
 - [87] S. Klimenko, G. Vedovato, M. Drago, F. Salemi, V. Tiwari, G. A. Prodi, C. Lazzaro, K. Ackley, S. Tiwari, C. F. Da Silva, and G. Mitselmakher, Method for detection and reconstruction of gravitational wave transients with networks of advanced detectors, *Phys. Rev. D* **93**, 042004 (2016).
 - [88] W. M. Farr, J. R. Gair, I. Mandel, and C. Cutler, Counting and confusion: Bayesian rate estimation with multiple populations, *Phys. Rev. D* **91**, 023005 (2015), arXiv:1302.5341 [astro-ph.IM].
 - [89] S. J. Kapadia, S. Caudill, J. D. E. Creighton, W. M. Farr, G. Mendell, A. Weinstein, K. Cannon, H. Fong, P. Godwin, R. K. L. Lo, R. Magee, D. Meacher, C. Messick, S. R. Mohite, D. Mukherjee, and S. Sachdev, A self-consistent method to estimate the rate of compact binary coalescences with a Poisson mixture model, *Classical and Quantum Gravity* **37**, 045007 (2020), arXiv:1903.06881 [astro-ph.HE].
 - [90] S. M. Gaebel, J. Veitch, T. Dent, and W. M. Farr, Digging the population of compact binary mergers out of the noise, *MNRAS* **484**, 4008 (2019), arXiv:1809.03815 [astro-ph.IM].

- [91] W. M. Farr, J. R. Gair, I. Mandel, and C. Cutler, Counting and confusion: Bayesian rate estimation with multiple populations, *Phys. Rev. D* **91**, 023005 (2015), arXiv:1302.5341 [astro-ph.IM].
- [92] S. M. Gaebel, J. Veitch, T. Dent, and W. M. Farr, Digging the population of compact binary mergers out of the noise, *MNRAS* **484**, 4008 (2019), arXiv:1809.03815 [astro-ph.IM].
- [93] S. Galadage, C. Talbot, and E. Thrane, Gravitational-wave inference in the catalog era: Evolving priors and marginal events, *Phys. Rev. D* **102**, 083026 (2020), arXiv:1912.09708 [astro-ph.HE].
- [94] T. Adams, D. Buskulic, V. Germain, G. M. Guidi, F. Marion, M. Montani, B. Mours, F. Piergiovanni, and G. Wang, Low-latency analysis pipeline for compact binary coalescences in the advanced gravitational wave detector era, *Classical and Quantum Gravity* **33**, 175012 (2016).
- [95] The LIGO Scientific Collaboration, the Virgo Collaboration, R. Abbott, T. D. Abbott, S. Abraham, F. Acernese, K. Ackley, C. Adams, R. X. Adhikari, V. B. Adya, and et al., Open data from the first and second observing runs of Advanced LIGO and Advanced Virgo, arXiv e-prints , arXiv:1912.11716 (2019), arXiv:1912.11716 [gr-qc].
- [96] G. Ashton, M. Hübner, P. Lasky, and C. Talbot, Bilby: A User-Friendly Bayesian Inference Library (2019).
- [97] G. Ashton, I. Romero-Shaw, C. Talbot, C. Hoy, and S. Galadage, bilby pipe: 1.0.1 (2020).
- [98] J. S. Speagle, DYNESTY: a dynamic nested sampling package for estimating Bayesian posteriors and evidences, *MNRAS* **493**, 3132 (2020), arXiv:1904.02180 [astro-ph.IM].
- [99] J. Skilling, Nested Sampling, in *Bayesian Inference and Maximum Entropy Methods in Science and Engineering: 24th International Workshop on Bayesian Inference and Maximum Entropy Methods in Science and Engineering*, American Institute of Physics Conference Series, Vol. 735, edited by R. Fischer, R. Preuss, and U. V. Toussaint (2004) pp. 395–405.
- [100] J. Skilling, Nested sampling for general Bayesian computation, *Bayesian Analysis* **1**, 833 (2006).
- [101] G. Ashton, M. Hübner, P. D. Lasky, C. Talbot, K. Ackley, S. Biscoveanu, Q. Chu, A. Divakarla, P. J. Easter, B. Goncharov, F. Hernandez Vivanco, J. Harms, M. E. Lower, G. D. Meadors, D. Melchor, E. Payne, M. D. Pitkin, J. Powell, N. Sarin, R. J. E. Smith, and E. Thrane, BILBY: A User-friendly Bayesian Inference Library for Gravitational-wave Astronomy, *ApJS* **241**, 27 (2019), arXiv:1811.02042 [astro-ph.IM].
- [102] R. J. E. Smith, G. Ashton, A. Vajpeyi, and C. Talbot, Massively parallel Bayesian inference for transient gravitational-wave astronomy, *MNRAS* **498**, 4492 (2020), arXiv:1909.11873 [gr-qc].
- [103] E. Thrane and C. Talbot, An introduction to Bayesian inference in gravitational-wave astronomy: Parameter estimation, model selection, and hierarchical models, *PASA* **36**, e010 (2019), arXiv:1809.02293 [astro-ph.IM].
- [104] I. M. Romero-Shaw, C. Talbot, S. Biscoveanu, V. D’Emilio, G. Ashton, *et al.*, Bayesian inference for compact binary coalescences with BILBY: validation and application to the first LIGO-Virgo gravitational-wave transient catalogue, *MNRAS* **499**, 3295 (2020), arXiv:2006.00714 [astro-ph.IM].
- [105] S. Khan, S. Husa, M. Hannam, F. Ohme, M. Pürrer, X. J. Forteza, and A. Bohé, Frequency-domain gravitational waves from nonprecessing black-hole binaries. II. A phenomenological model for the advanced detector era, *Physical Review D* **93**, 044007 (2016).
- [106] S. Ossokine, A. Buonanno, S. Marsat, R. Cotesta, S. Babak, T. Dietrich, R. Haas, I. Hinder, H. P. Pfeiffer, M. Pürrer, C. J. Woodford, M. Boyle, L. E. Kidder, M. A. Scheel, and B. Szilágyi, Multipolar effective-one-body waveforms for precessing binary black holes: Construction and validation, *Phys. Rev. D* **102**, 044055 (2020), arXiv:2004.09442 [gr-qc].
- [107] B. P. Abbott, R. Abbott, T. D. Abbott, *et al.*, A guide to LIGO-Virgo detector noise and extraction of transient gravitational-wave signals, arXiv e-prints , arXiv:1908.11170 (2019), arXiv:1908.11170 [gr-qc].
- [108] C. Talbot and E. Thrane, Gravitational-wave astronomy with an uncertain noise power spectral density, arXiv e-prints , arXiv:2006.05292 (2020), arXiv:2006.05292 [astro-ph.IM].
- [109] K. Chatziioannou, C.-J. Haster, T. B. Littenberg, W. M. Farr, S. Ghonge, M. Millhouse, J. A. Clark, and N. Cornish, Noise spectral estimation methods and their impact on gravitational wave measurement of compact binary mergers, *Phys. Rev. D* **100**, 104004 (2019).
- [110] S. Biscoveanu, C.-J. Haster, S. Vitale, and J. Davies, Quantifying the effect of power spectral density uncertainty on gravitational-wave parameter estimation for compact binary sources, *Phys. Rev. D* **102**, 023008 (2020), arXiv:2004.05149 [astro-ph.HE].
- [111] D. Macleod, A. L. Urban, S. Coughlin, T. Massinger, M. Pitkin, paulaltin, J. Areeda, E. Quintero, T. G. Badger, L. Singer, and K. Leinweber, gwpy/gwpy: 1.0.1 (2020).
- [112] S. E. Woosley and A. Heger, The Pair-Instability Mass Gap for Black Holes, arXiv e-prints , arXiv:2103.07933 (2021), arXiv:2103.07933 [astro-ph.SR].
- [113] A. Heger and S. E. Woosley, The Nucleosynthetic Signature of Population III, *ApJ* **567**, 532 (2002), arXiv:astro-ph/0107037 [astro-ph].
- [114] Carbonfund.org, Carbon Fund (2020).